Robust Hybrid Beamforming Design for Multi-RIS Assisted MIMO System with Imperfect CSI

Zhen Chen, *Member, IEEE,* Jie Tang, *Senior Member, IEEE,* Xiu Yin Zhang, *Fellow, IEEE,* Qingqing Wu, *Senior Member, IEEE,* Gaojie Chen, *Senior Member, IEEE,* and Kai-Kit Wong, *Fellow, IEEE*

***Abstract*—Reconfigurable intelligent surface (RIS) has been developed as a promising approach to enhance the performance of fifth-generation (5G) systems through intelligently reconfiguring the reflection elements. However, RIS-assisted beamforming design highly depends on the channel state information (CSI) and RIS's location, which could have a significant impact on system performance. In this paper, the robust beamforming design is investigated for a RIS-assisted multiuser millimeter wave system with imperfect CSI, where the weighted sum-rate maximization problem (WSM) is formulated to jointly optimize transmit beamforming of the BS, RIS placement and reflect beamforming of the RIS. The considered WSM maximization problem includes CSI error, phase shifts matrices, transmit beamforming as well as RIS placement variables, which results in a complicated nonconvex problem. To handle this problem, the original problem is divided into a series of subproblems, where the location of RIS, transmit/reflect beamforming and CSI error are optimized iteratively. Then, a multiobjective evolutionary algorithm is introduced to gradient projection-based alternating optimization, which can alleviate the performance loss caused by the effect of imperfect CSI. Simulation results reveal that the proposed scheme can potentially enhance the performance of existing wireless communication, especially considering a desirable trade-off among beamforming gain, user priority and error factor.**

***Index Terms*—Reconfigurable intelligent surface, imperfect channel state information, RIS placement optimization, beamforming design, non-convex optimization.**

This work was supported in part by the National Key Research and Development Project under Grant 2019YFB1804100, in part by the National Natural Science Foundation of China under Grant 62001171, 61971194, 62222105, in part by the Engineering and Physical Sciences Research Council (EPSRC) under grant EP/V052942/1, in part by the Natural Science Foundation of Guangdong Province under Grant 2021A1515011966, 2022A1515011189, in part by the Open Research Fund of State Key Laboratory of Integrated Services Networks, Xidian University (No. ISN23-05). (*Corresponding author: Jie Tang*.)

Z. Chen is with the School of Electronic and Information Engineering, Shenzhen University, Shenzhen, China, and also with State Key Laboratory of Integrated Service Networks, Xidian University, Xi'an 210096, China. (e-mail:chenz.scut@gmail.com).

J. Tang is with the School of Electronic and Information Engineering, South China University of Technology, Guangzhou, China. (e-mail: eejtang@scut.edu.cn).

X. Zhang is with the Engineering Research Center of Short-Distance Wireless Communications and Network, Ministry of Education, and also with School of Electronic and Information Engineering, South China University of Technology, Guangzhou, China. (e-mail: zhangxiuyin@scut.edu.cn).

Q. Wu is with the Department of Electronic Engineering, Shanghai Jiao Tong University, 200240, China (e-mail: wu.qq1010@gmail.com).

G. Chen is with the Institute for Communication Systems (ICS), 5GIC & 6GIC, University of Surrey, Guildford, Surrey GU2 7XH, U.K. (e-mail: gaojie.chen@surrey.ac.uk).

K.-K Wong is with the Department of Electronic and Electrical Engineering, University College London, London, United Kingdom. (e-mail: kaikit.wong@ucl.ac.uk).

I. Introduction

MILLIMETER (mmWave) techniques have the potential of supporting high spectral efficiency (SE) by exploiting highly directional beamforming [1]. However, since directional mmWave links are highly susceptible to blockage, a large number of active antenna arrays and radio-frequency chains are required, which may lead to excessive circuit energy consumption and hardware cost. To reduce the hardware cost of system, reconfigurable intelligent surface (RIS), as a promising technology, has great potential to improve the performance of beyond fifth-generation (5G) and sixth-generation (6G) network [2]. Specifically, RIS is made of a newly developed metamaterial, which can establish a favourable transmission environment by collaboratively adjusting amplitude and phase shift (PS) to improve the spectral and energy efficiency [3]. It is worth noting that the RIS only consists of low-cost passive reflecting elements, which differs significantly from the conventional amplify-and-forward relay [4]. More importantly, low hardware footprints of RIS structures promote low implementation cost, high-flexibility, and hence they can be easily deployed and integrated into existing wireless communication systems without changing the existing infrastructure and operating standards [5]. Therefore, the design of RIS in assisting wireless communications has attracted extensive attention in both industrial and academia.

Due to the significant potentials posed by the RIS, various RIS-assisted wireless communications were extensively studied, such as passive beamforming designs [6]–[9], RIS-assisted channel estimation [10] and so on. Particularly, the authors in [11] exploited RIS to control the wireless propagation environment and enhance the coverage and transmission rate. To study the suitability of RIS in terms of the SE, a jointly optimizing the active/transmit beamforming (ABF) and passive/reflect beamforming (PBF) was developed to minimize the transmission power of system with respect to the signal-to-interference-plus-noise (SINR) constraints [12]. The studies in [13] exploited the maximum-ratio transmission scheme for RIS-assisted single-cell wireless system, where a joint PBF and ABF optimization problem was formulated. Also, a similar problem was considered for multiple RIS-assisted systems, which jointly optimize the ABF at the BS and the PBF at the RIS to improve robustness against blockages [14]. In [15], the authors investigated energy-efficiency maximization approach for RIS-based downlink multi-user MISO system. Subsequently, authors further develop holographic MIMO surfaces for diverse wireless communication applications [16]. Besides, the

authors in [17] investigated an artificial noise-aided secure MIMO communication system by exploiting RIS to enhance the physical layer security. Moreover, RIS was also applied as an auxiliary facility to support secret wireless communication, wireless information and power transfer, integrated sensing and communication and unmanned aerial vehicle (UAV) communications [18]–[24].

However, the performance of RIS-assisted communication depends on the adaptivity of the reflecting elements. In general, the choice of RIS positions is initially oriented towards the BS, since this leads to a lower path loss. If some of the blockages are still present, the RIS's location are slightly adjusted, and then abundant reconfigurable reflecting elements should be further trained. One of the major concerns is how to rapidly tune the RIS's phase shifts to realize the signal transmission. In particular, the channel state information (CSI) varies over time in mobility transmission scenarios, and thus it is difficult to perform RIS phase shifts tuning by employing full CSI. It is worth noting that most of the research on the throughput gain in RIS-assisted communication systems focus on the performance analysis [25]–[27]. Only a few involves the optimization problem of RIS-assisted optimization problem. However, optimization for RIS-assisted communication system is critically dependent on the availability of perfect CSI. Furthermore, considering mobility scenarios with fast time-varying channels, the transmitters may only be able to obtain partial or outdated CSI, which inevitably results in the signal misalignment in RIS-assisted wireless networks. Therefore, considering the imperfect CSI for robust beamforming design of optimization problem could be further investigated.

To ensure the service quality, more efforts were dedicated to the RIS-assisted beamforming design with imperfect CSI [28]–[30]. In [30], a RIS-assisted vertical beamforming scheme for cognitive radio networks were proposed by jointly optimizing the beamforming vector, tilt angle as well as the phase shifts. The work of [31] investigated a worst-case beamforming design for a multi-user MISO wireless system, where the CSI was assumed to be imperfect. In addition, the large-scale of RISs were also deployed in hybrid wireless network, where the passive beamforming was presented to improve the spectral and energy efficiency by tuning massive low-cost passive reflecting elements [32]. In fact, it was more practical to consider the cascaded channel uncertainty in RIS-assisted wireless systems. To this end, Zhou *et. al* [33] investigated a robust secure transmission framework with cascaded channel error in secure RIS-assisted communication systems. However, considering the bandwidth with limited feedback, the transmitters lack perfect CSI feedback. In particular, to reduce the hardware cost, RIS was generally not equipped with any transmitter module and thus not capable of performing any baseband processing functionality [34]. This will inevitably lead to channel estimation error for exiting beamforming design.

Motivated by the above observations, the robust beamforming design with imperfect CSI for RIS-assisted wireless communication is still in its infancy and needs to be further discussed in the open literature.

- *First, in mobility transmission scenarios, CSI has to be re-estimated and the phase shifts of all the elements has to be adjusted frequently, thus incurring significant channel training overhead and beamforming design complexity [35]. Therefore, the design of robust beamforming under imperfect CSI should be considered for RIS-assisted system.*
- *Second, to realize phase tuning in practice, RIS is equipped with smart controllers that is used to adjusting the biasing voltages according to the available CSI [36]. It is worth noting that the reflecting elements do not require radio frequency (RF) chains to avoid additional transmit power consumption ideally, but continuous operations to the smart controller will still be power-consuming. In practice, the corresponding number of RIS elements can be quite large, which becomes a significant obstacle to obtain the accurate CSI.*
- *Finally, since each transmission link has distinct number of data streams and undergoes different reflecting pathes between BS-RIS and RIS-UE channel, the placement of RIS affects each transmission channel. Therefore, finding an appropriate place for RIS can further improve the communication performance, which is imperative to take the placement optimization and CSI error into consideration when designing the RIS-assisted beamforming scheme.*

As a result, how to jointly optimize the RIS-assisted beamforming, RIS placement as well as the CSI error becomes a challenging issue. To this end, we propose the design of robust beamforming framework for RIS-assisted wireless communications under imperfect CSI, where CSI error, the placement of RIS, phase shifts matrices and transmit beamforming can be flexibly determined to enhance the system performance. The major contributions of this paper can be summarized as follows.

1) A robust beamforming scheme is proposed in the multi-RIS assisted MIMO system, where the phase shifts of RIS, CSI error the RIS placement and transmit beamforming are jointly optimized to improve the beamforming gain. To improve the robustness of beam design, the RIS is composed of multiple RIS units, which can avoid beam misalignment caused by parts reflecting element broken. According to the proposed framework, a joint beamforming optimization problem is formulated to maximize the SE, subject to CSI error, transmit beamforming, RIS placement and phase shifts constraints on multi-RIS reflecting elements.
2) The proposed optimization problem for robust beamforming design is non-convex due to the fact that multiple variables are strongly coupled together, which makes it difficult to solve directly. To tackle this issue, we transform the beamforming optimization problem into an equivalent yet more tractable form. Based on it, an efficient gradient projection (GP)-based multiobjective evolutionary algorithm (GP-MEA) is developed to solve the optimization problem, which can converge to the Pareto set.
3) To suppress the CSI error caused by unsuspected feed-

This article has been accepted for publication in IEEE Transactions on Wireless Communications. This is the author's version which has not been fully edited and content may change prior to final publication. Citation information: DOI 10.1109/TWC.2022.3222218

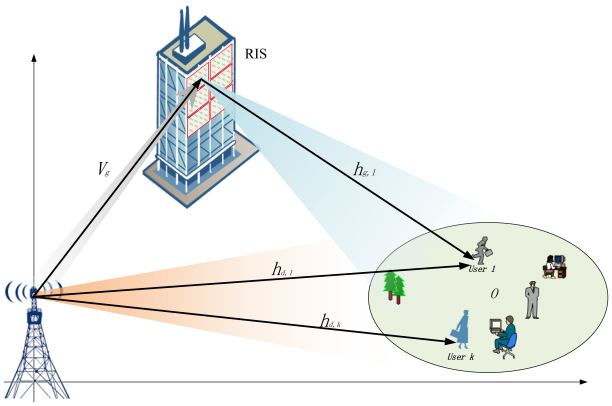

Fig. 1. Illustration of the considered multi-RIS-assisted MIMO communication system.

back delay or the effect of the RIS, we transform the CSI error subproblem into a multiobjective optimization problem and develop a novel evolutionary algorithm algorithm based on decomposition (MOEA/D) to adjust the beamforming gain, the priority and error factor. We also verify that this scheme is superior to conventional schemes in maximum beamforming gain, the priority and minimum error factor to achieve multi-object optimum.

4) The effectiveness of the proposed beamforming scheme is validated by extensive simulation results, which illustrate that the proposed mechanism and the corresponding algorithm can improve the SE significantly over the conventional beamforming design. Moreover, the proposed mechanism could provide useful insights into the robust beamforming design on effects of the RIS placement and CSI error.

A. Organization and Notations

The remainder of this article is arranged as follow. Section II presents the system model and formulates the corresponding joint optimization problem. In Section III, the joint optimization of transmit beamforming, CSI error, RIS placement and phase shifts of RIS are studied in detail. In Section IV, the proposed GP-MEA algorithm is exploited to solve the proposed problem under imperfect CSI. Simulation results and discussions are provided to verify the effectiveness of the proposed mechanism in Section V, which is followed by conclusions in Section VI.

Notations: $\mathbb{C}$ represents the set of complex numbers; vector is denoted by bold-face lower-case letters; upper-case boldface letters represent matrix; ∂ represents the gradient; $(\cdot)^T$, and $(\cdot)^H$ refer to the transpose, and the conjugate transpose of the vector, respectively; $\boldsymbol{I}$ and $\mathrm{tr}(\cdot)$ denote an identity matrix and trace of matrix, $\mathrm{vec}(\cdot)$ and $\mathrm{diag}(\cdot)$ denote the vectorization and diagonalization; $\otimes$ is denoted as the Kronecker product; $\mathbb{E}\{\cdot\}$ represents the statistical expectation operator and $[\cdot]_{i,j}$ denotes the (i,j)-th entry of a matrix.

II. System Model and Problem Formulation

In this section, we follow the system model of current state-of-the-art works on RIS-assisted MIMO system [12]–[14], in which RIS is deployed between BS and UEs. The joint design of transmit beamforming of the BS, phase shift of the RIS, the optimal placement of RIS and the CSI error are constructed to maximize the SE performance of system.

A. RIS-assisted Communication Scenario

Considering a muti-RIS assisted MIMO system, a multi-antenna BS is deployed to serve K single-antenna UEs. As shown in Fig. 1, RIS equipped with G RIS units is deployed to enhance the communication coverage, which are located in the altitude H_{RIS}. This design can avoid partly reflecting element of RIS broken that affect the exact CSI requirement. Each RIS unit is arranged in the form of an $M = M_{\mathrm{az}} \times M_{\mathrm{el}}$ rectangular array with M_{az} elements horizontally and M_{el} elements vertically, which are controlled by a smart controller to coordinate the reflecting modes. The BS is deployed at a fixed altitude H_{BS}, which is located in the coordinates $\boldsymbol{o}_{BS} = (0,0)$. For simplicity, we set the altitude H_{BS} to be $H_{BS} = 2H_{RIS}$. All UEs are placed in the circular coordinate area, which is the coverage area of passive beam. The center of the coverage area is denoted by $\boldsymbol{o}_o = [o_o(1), o_o(2)]^T$. The location of the UE can be specified as $\boldsymbol{o}_{UE} = [o_{UE}(1), o_{UE}(2)]^T$, where $\{o_{UE}(1), o_{UE}(2)\}$ satisfies $(o_o(1)-o_{UE}(1))^2+(o_o(2)-o_{UE}(2))^2 \leq r^2$ and r denotes the radius of the coverage area. As shown in Fig. 2, the RIS unit is small than RIS and the size of RIS units are much less than the distance between RIS and users. Thus, the differences between different RIS unit and the center of the coverage area are ignored. Then, the first reflecting element of g-th RIS is regarded as a reference position and the horizontal and vertical location of the reference position is denoted by $\boldsymbol{o}_{RIS_g} = (o_{RIS_g}(1), o_{RIS_g}(2))$. Then, the distance between the BS and k-th UE is expressed as $d_{BU,k} = \sqrt{H_{BS}^2 + \|\boldsymbol{o}_{BS} - \boldsymbol{o}_{UE_k}\|_2^2}$, $k = 1, ..., K$. Similarly, the distance between the g-th RIS and the UEs are expressed as $d_{IU,k} = \sqrt{H_{RIS_g}^2 + \|\boldsymbol{o}_{RIS_g} - \boldsymbol{o}_{UE_k}\|_2^2}$, $k = 1, ..., K$. We assume that the coverage area of beam is the circular coordinate area and all UEs are placed in this circular coordinate area. Then, the center location of the coverage area $\boldsymbol{o}_o$ is used in place of $\boldsymbol{o}_{UE}$.

B. RIS Design with Limited Reflection Elements

Let $\boldsymbol{\Theta} = [\boldsymbol{\Theta}_1\ \boldsymbol{\Theta}_2\ , ...,\ \boldsymbol{\Theta}_G]$ be the reflection coefficient matrix for the RIS, reflecting coefficient matrix of each RIS unit is given by

$$\boldsymbol{\Theta}_g = \mathrm{diag}\{\theta_{g,1}, \theta_{g,2}, ..., \theta_{g,M}\}, \quad g \in \{1, ..., G\}, \tag{1}$$

where $\theta_{g,i}$ is i-th reflecting element of g-th RIS unit and the reflecting elements $\{\theta_{g,i}\}$ are assumed to be continuously controllable. According to (1), the setting of the reflecting elements are considered in the following two cases.

1) Ideal RIS: The reflecting elements are updated by using arbitrary amplitudes and phase shifts. Thus, the feasible set of $\theta_{g,i}$ can be formulated as

$$\mathcal{F}_1 = \{\theta_{g,i} | |\theta_{g,i}|^2 \in [0,1]\}. \tag{2}$$

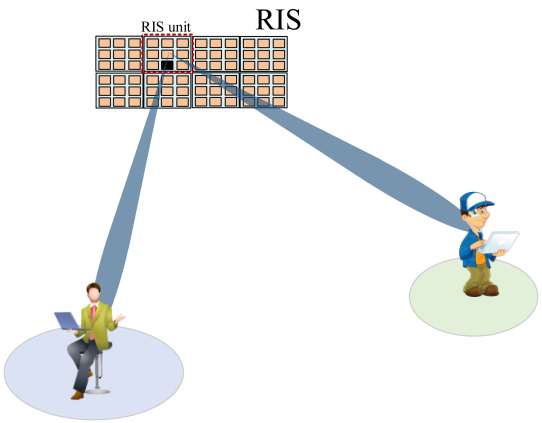

Fig. 2. Illustration of the multi-RIS-assisted beamforming design under partial reflecting element of RIS broken case.

2) Non-ideal RIS: The reflecting amplitude of RIS is designed as a fixed value, such as $\varsigma = 1$. For this scenario, the design of PSs consists of two cases, namely continuous PSs and discrete PSs. To be specific, the feasible set of $\theta_{g,i}$ is exploited for continuous phase shifts, which can be formulated as

$$\mathcal{F}_2 = \left\{\theta_{g,i} | \theta_{g,i} = \varsigma e^{j\varphi_{g,i}}, \varphi_{g,i} \in [0, 2\pi), \varsigma = 1\right\} \tag{3}$$

and the discrete PSs set $\{\theta_{g,i}\}$ with B resolution bits can be formulated as

$$\mathcal{F}_3 = \left\{\theta_{g,i} | \theta_{g,i} = \varsigma e^{j\varphi_{g,i}}, \varphi_{g,i} \in \mathcal{D}, \varsigma = 1\right\}, \tag{4}$$

where the codebook $\mathcal{D} = \left\{\frac{2\pi n}{2^B}, n = 1, 2, ..., 2^B\right\}$.

C. RIS-assisted Channel Model

In this subsection, RIS-assisted channel model is discussed, where the baseband equivalent channel is comprised of BS-UE, BS-RIS and RIS-UE link, respectively. Since fixed location of the BS facilitate accurate CSI, the channel from the BS to the RIS (BS-RIS link) is assumed to be an line-of-sight (LoS) channel, where the RIS is commonly placed on the facade of an buildings. Due to the insufficient angular spread of the scattering environment, BS-RIS and RIS-UE channels can be modeled by a Rician fading channel [37]. To facilitate RIS channel estimation, the BS-RIS and RIS-UE links are collectively called the BS-RIS-UE link. Meanwhile, the Rayleigh fading channel model is used betwwen the BS and UE link. Even if the signal transmitted through the BS-UE link suffers from blockage, there still exist extensive scatters. For the BS-UE link of the k-th UE, $\boldsymbol{h}_{d,k}$ can be expressed as

$$\boldsymbol{h}_{d,k} = \sqrt{\rho d_{BU,k}^{-\kappa}} \boldsymbol{h}_{BU,k}, \tag{5}$$

where ρ is the path loss between the BS and UE at the reference distance of 1 meter [38], κ is the corresponding path loss exponent related to the BS-UE channel, $d_{BU,k}$ denotes the distance between the BS and the k-th UE, and $\boldsymbol{h}_{BU,k}$ denotes the random scattering component modeled with real and imaginary parts independent and identically distributed zero mean random variables.

According to [12], the BS to the RIS channels are mainly dominated by the *LoS* links. Thus, the BS-RIS$_g$ channel in the g-th RIS units, denoted by $\boldsymbol{V}_g \in \mathbb{C}^{M \times N}$, is given by

$$\boldsymbol{V}_g = \sqrt{\rho d_{BI}^{-2}} \hat{\boldsymbol{V}}_g = \sqrt{\rho d_{BI}^{-2}} \mathbf{a}(\nu_{t,g}) \mathbf{a}(\nu_{r,g}), \tag{6}$$

where $d_{BI} = \sqrt{(H_{BS} - H_{RIS_g})^2 + \|\boldsymbol{o}_{RIS_g} - \boldsymbol{o}_{BS}\|_2^2}$ denotes the distance from the BS to the g-th RIS. The steering vector $\mathbf{a}(\nu_{t,g})$, $\mathbf{a}(\nu_{r,g})$ can be defined as

$$\begin{aligned} \mathbf{a}(\nu_{t,g}) &= \left[1, e^{\frac{j2\pi\ell_x}{\lambda}\nu_{t,g}}, ..., e^{\frac{j2\pi\ell_x}{\lambda}\nu_{t,g}(N-1)}\right]^T, \\ \mathbf{a}(\nu_{r,g}) &= \left[1, e^{\frac{j2\pi\ell_x}{\lambda}\nu_{r,g}}, ..., e^{\frac{j2\pi\ell_x}{\lambda}\nu_{r,g}(M-1)}\right]^T, \end{aligned} \tag{7}$$

where $j = \sqrt{-1}$, $\nu_{t,g}$ and $\nu_{r,g}$ represent the cosine of angle-of-arrival (AoA) and angle-of-departure (AoD), respectively. ℓ_x denotes the antenna spacing and parameter λ represents the carrier wavelength of signal.

Similarly, by employing the Rician fading model, the RIS-UE channel of the k-th UE is modeled as $\boldsymbol{h}_{g,k} \in \mathbb{C}^{M \times 1}$, which can be expressed as [39]

$$\boldsymbol{h}_{g,k} = \sqrt{\rho d_{IU,k}^{-2}} \hat{\boldsymbol{h}}_{g,k} = \sqrt{\rho d_{IU,k}^{-2}} \left(\sqrt{\frac{\beta}{\beta+1}} \boldsymbol{h}_{IU,k}^{LoS} + \sqrt{\frac{1}{\beta+1}} \boldsymbol{h}_{IU,k}^{NLoS}\right), \tag{8}$$

where $d_{IU,k}$ denotes the distance between the RIS and the k-th UE; β is the Rician factor. The deterministic *LoS* channel is expressed as $\boldsymbol{h}_{IU,k}^{LoS} = \left[1, e^{\frac{j2\pi\ell_x}{\lambda}\vartheta_{r,k}}, ..., e^{\frac{j2\pi\ell_x}{\lambda}\vartheta_{r,k}(M-1)}\right]^T \in \mathbb{C}^{M \times 1}$ and the non-LoS (*NLoS*) channel $\boldsymbol{h}_{IU,k}^{NLoS} \in \mathbb{C}^{M \times 1}$ with zero-mean and unit-variance circularly symmetric complex Gaussian (CSCG) random variable.

Based on the above channel model, above channel structure can be applied to design the RIS-assisted beamforming. As mentioned earlier, however, previous works only consider the beamforming design for a fixed RIS location/deployment and perfect CSI, which cannot be directly applied to RIS-assisted mmWave systems. In hope of seeking a high quality suboptimal solution, we will investigate how imperfect CSI can be utilized to design robust hybrid beamforming scheme in the following section.

III. RIS-assisted Beamforming Design and Problem Formulation

A. Problem Formulation and Transformation

In this section, to realize reflected signals toward preferable directions, we investigate the robust beamforming scheme for RIS-assisted communication, where the transmit beamforming of the BS is performed while the reflect beamforming is achieved by optimizing the phase shifts of RIS. From a systematic perspective, we formulate the spectral efficiency of the maximization problem as our design criterion, and then decompose it into the transmit beamforming, CSI error, RIS placement and the phase shifts of RIS subproblems.

Let s_k be the transmitted symbol of the k-th UE with zero mean and unit variance. Thus, corresponding to the complex baseband signal $\boldsymbol{x}$ at the BS can be written as

$$\boldsymbol{x} = \sum_{k=1}^{K} \boldsymbol{w}_k s_k, \tag{9}$$

where $\boldsymbol{w}_k \in \mathbb{C}^N$ denotes the active beamforming vector for the k-th UE. Based on this, the k-th received signal of the UE can be represented as

$$\begin{aligned} \hat{\mathrm{y}}_k &= \boldsymbol{h}_{d,k}^H \boldsymbol{x} + \sum_{g=1}^{G} \boldsymbol{h}_{g,k}^H \boldsymbol{\Theta}_g \boldsymbol{V}_g \boldsymbol{x} + n_k, \\ &= \left(\boldsymbol{h}_{d,k}^H + \sum_{g=1}^{G} \boldsymbol{h}_{g,k}^H \boldsymbol{\Theta}_g \boldsymbol{V}_g \right) \sum_{k=1}^{K} \boldsymbol{w}_k s_k + n_k, \end{aligned} \tag{10}$$

where $n_k \sim \mathcal{CN}(0, \sigma^2)$ denotes the additive complex Gaussian noise with zero mean and variance σ^2. To make the above expression (10) more tractable, we further define $\boldsymbol{\theta}_g = \mathrm{vec}(\mathrm{diag}(\boldsymbol{\Theta}_g))$ and the cascade channel $\boldsymbol{h}_{g,k}^H \boldsymbol{\Theta}_g \boldsymbol{V}_g$ can be rewritten as $\boldsymbol{\theta}_g^H \boldsymbol{H}_{g,k}$, where $\boldsymbol{H}_{g,k} = \sqrt{d_{IU,k}^{-2}} \mathrm{diag}(\hat{\boldsymbol{h}}_{g,k}^H) \boldsymbol{V}_g = \mathrm{diag}(\boldsymbol{h}_{g,k}^H) \boldsymbol{V}_g$ and then the received signal s_k of the k-th UE is equivalently rewritten as

$$\hat{s}_k = \left(\boldsymbol{h}_{d,k}^H + \sum_{g=1}^{G} \boldsymbol{\theta}_g^H \boldsymbol{H}_{g,k} \right) \sum_{k=1}^{K} \boldsymbol{w}_k s_k + n_k. \tag{11}$$

Since the CSI is sensitive to unsuspected feedback delay or the effect of the RIS, the residual CSI error will substantially impact the overall system performance due to imperfect CSI [40], [41]. Moreover, partial reflecting element of RIS broken that affect the exact CSI requirement. Although we consider simple Rayleigh fading channels for RIS-assisted syatem, it is still difficult to estimate the accurate channel. Based on above observation and characteristics of mmWave channel, the transmitters have imperfect CSI $\hat{\boldsymbol{h}}_k$, and the relation between the perfect and the imperfect CSI can be expressed as [42]

$$\hat{\boldsymbol{h}}_k = \sqrt{1-\zeta_k} \boldsymbol{h}_k + \sqrt{\zeta_k} \boldsymbol{h}_{e,k} \tag{12}$$

where $\boldsymbol{h}_k^H = \boldsymbol{h}_{d,k}^H + \sum_{g=1}^{G} \boldsymbol{\theta}_g^H \boldsymbol{H}_{g,k}$ denotes the perfect channel of the k-th UE and $\boldsymbol{h}_{e,k}$ is the corresponding residual CSI error with i.i.d. zero-mean and unit-variance complex Gaussian entries, and is independent of $\boldsymbol{h}_k$. ζ_k denotes the error factor, scaling from 0 to 1 , indicates the CSI accuracy. If $\zeta_k = 0$, then k-th UE has perfect CSI. Intuitively, ζ_k is related to the unsuspected feedback delay or the CSI exchange amount B and can be approximated as 2^B. If the CSI exchange amount tends to infinity, the transmitter can obtain perfect CSI. Considering the issue of imperfect CSI, we introduce the estimation error to model the channel, and then the received signal at the k-th UE is written as

$$\begin{aligned} \hat{s}_k = &\underbrace{\sqrt{1-\zeta_k} \boldsymbol{h}_k^H \boldsymbol{w}_k s_k}_{\text{desired signal}} + \underbrace{\sqrt{\zeta_k} \boldsymbol{h}_{e,k}^H \boldsymbol{w}_k s_k}_{\text{residual CSI error}} \\ &+ \underbrace{\sqrt{1-\zeta_k} \boldsymbol{h}_k^H \sum_{k \neq i}^{K-1} \boldsymbol{w}_i s_i}_{\text{multiuser interference}} + \underbrace{n_k}_{\text{noise}}. \end{aligned} \tag{13}$$

To maximize the SE of system, the corresponding SINR of the k-th UE is given by

$$\gamma_k = \frac{\left| \sqrt{1-\zeta_k} \left(\boldsymbol{h}_{d,k}^H + \sum_{g=1}^{G} \boldsymbol{\theta}_g^H \boldsymbol{H}_{g,k} \right) \boldsymbol{w}_k \right|^2}{\sum_{i=1, i \neq k}^{K} \left| \sqrt{1-\zeta_k} \left(\boldsymbol{h}_{d,k}^H + \sum_{g=1}^{G} \boldsymbol{\theta}_g^H \boldsymbol{H}_{g,k} \right) \boldsymbol{w}_i \right|^2 + \left| \sqrt{\zeta_k} \boldsymbol{h}_{e,k}^H \boldsymbol{w}_k \right|^2 + \sigma^2} \tag{14}$$

with

$$\sum_{k=1}^{K} \|\boldsymbol{w}_k\|_2^2 \leq P_{\max} \tag{15}$$

being the power constraint associated with BS, where $P_{\max}$ denotes the maximum transmit power. In general, the k-th UE treats the transmit signal from other UEs (*i.e.*, $s_1, ..., s_{k-1}, s_{k+1}, ..., s_K$) as interference.

Accordingly, the achievable SE r_k of k-th UE can be formulated as (16), which can be given by the top of the next page. where ω_k denotes the priority for k-th UE. Based on the SINR principle, it is observed that the SE of (16) in a specific cell is coupled with transmit beamforming, RIS placement, CSI error and phase shifts matrices. To make the problem tractable, the weighted sum-rate maximization (WSM) of the proposed RIS-assisted mmWave system is adopted as the design criterion. As a consequence, we strive to jointly optimize the phase shifts matrices, transmit beamforming of the BS, RIS placement and CSI error to improve the SE performance. Based on (14) and (16), the considered optimization problem can be formulated as

$$\mathcal{P}(A1) \max_{\boldsymbol{o}_{RIS}, \boldsymbol{W}, \boldsymbol{\theta}_g, \boldsymbol{\zeta}} \left\{ f_{A1}\left(\boldsymbol{o}_{RIS}, \boldsymbol{\theta}_g, \boldsymbol{W}, \boldsymbol{\zeta}\right) = \sum_{k=1}^{K} \omega_k \log_2(1+\gamma_k) \right\}, \tag{17a}$$

$$s.t. \sum_{k=1}^{K} \left(\boldsymbol{w}_k^H \boldsymbol{w}_k \right) \leq P_{\max}, \tag{17b}$$

$$\theta_{g,m} \in \mathcal{F}_c, \quad c = \{1, 2, 3\} \tag{17c}$$

where $\boldsymbol{W} = [\boldsymbol{w}_1, ..., \boldsymbol{w}_K]$, $\boldsymbol{\zeta} = [\zeta_1, ..., \zeta_K]$ and the phase shifts feasible set for $\theta_{g,m}$ is $\mathcal{F}_c$, which can be given by ideal RIS and non-ideal RIS cases.

It is obvious that the maximization problem $\mathcal{P}(A1)$ in (17) is challenging due to the following reasons. First, the objective function in (17a) makes $\mathcal{P}(A1)$ essentially a non-convex optimization problem because of the coupling of various optimization variables. Second, adjusting all reflecting elements of a large RIS in $\mathcal{P}(A1)$ with phase shifts operation is computationally expensive. Moreover, the presence of

$$r_k = \omega_k \log_2 \left(1 + \frac{\left| \sqrt{1-\zeta_k} \left(\boldsymbol{h}_{d,k}^H + \sum_{g=1}^{G} \boldsymbol{\theta}_g^H \boldsymbol{H}_{g,k} \right) \boldsymbol{w}_k \right|^2}{\sum_{i=1, i\neq k}^{K} \left| \sqrt{1-\zeta_k} \left(\boldsymbol{h}_{d,k}^H + \sum_{g=1}^{G} \boldsymbol{\theta}_g^H \boldsymbol{H}_{g,k} \right) \boldsymbol{w}_i \right|^2 + \left| \sqrt{\zeta_k} \boldsymbol{h}_{e,k}^H \boldsymbol{w}_k \right|^2 + \sigma^2} \right), \tag{16}$$

the power constraint (17b) and CSI error further complicate the optimization procedure. In the following, we develop an innovative scheme to solve these difficult problem.

IV. Solutions of the Optimization Problem

In this section, an alternating optimization strategy is a computationally efficient method for solving the above optimization problem. Nevertheless, considering the feasible solution involving four variables of problem (17) is nonconvex, which cannot guarantee that the solution obtained by this strategy is feasible. To tackle this issues, the problem $\mathcal{P}(A1)$ is equivalently translated into a more tractable form $\mathcal{P}(A2)$ by exploiting the fractional programming (FP) technique [28], [43]. Different from previous works, the introduction of CSI error and RIS placement will result in the phenomena of the slower convergence. To facilitate the convergence of the FP technique, the gradient projection strategy is integrated into phase shifts optimization processing. Subsequently, the joint beamforming optimization problem is divided into several subproblem that can be optimized by fixing the remaining variables, respectively. Moreover, the Proposition I is provided to show that the algorithm can carry out the stationary solution.

Firstly, the closed-form FP scheme is developed to solve the weighted sum-of-logarithms-of-ratio problem as follows

$$\max_{\boldsymbol{z}} \sum_{k=1}^{K} \omega_k \log_2 \left(1 + \frac{|A_k(\boldsymbol{z})|^2}{B_k(\boldsymbol{z}) - |A_k(\boldsymbol{z})|^2} \right), \tag{18}$$

where $|A_k(\boldsymbol{z})|$ is a nonnegative function, $B_k(\boldsymbol{z})$ is a positive function and $B_k(\boldsymbol{z}) > |A_k(\boldsymbol{z})|^2$ for all k. From the objective function of the problem (18), the ratio $\frac{|A_k(\boldsymbol{z})|^2}{B_k(\boldsymbol{z})-|A_k(\boldsymbol{z})|^2}$ can be physically regarded as the SINR term in (17a). The derivation process referred to the recent review [43] for details. To provide insight on how the closed form FP approach is obtained, the problem (18) is revisited by using the *Lagrangian dual transform* perspective, which can be divided into two stages:

According to [43], by introducing *Lagrangian dual transform*, the logarithm function $\log(1+\gamma_k)$ can be expressed as

$$\max_{\gamma_k, \alpha_k \geq 0} \omega_k \log(1+\alpha_k) - \omega_k \alpha_k + \omega_k \frac{(1+\alpha_k)\gamma_k}{1+\gamma_k}. \tag{19}$$

which can be equivalently transformed as

$$\max_{\boldsymbol{z}, \alpha} \sum_{k=1}^{K} \omega_k \log(1+\alpha_k) - \omega_k \alpha_k + \omega_k (1+\alpha_k) \frac{|A_k(\boldsymbol{z})|^2}{B_k(\boldsymbol{z})}, \tag{20a}$$

$$s.t. \quad \alpha_k \geq 0, \quad \forall k = 1, ..., K, \tag{20b}$$

where α_k is an auxiliary variable. It is pointed out in [43] that the maximization problem (20) is equivalent to the problem (18). Then, with the newly transformed objective function, the quadratic transform technique is introduced to deal with the FP problem.

Quadratic Transform: Given the variable $\boldsymbol{\alpha} = [\alpha_1, ..., \alpha_K]^T$, we focus on the optimization problem as follows

$$\max_{\boldsymbol{z}} \sum_{k=1}^{K} \frac{|A_k(\boldsymbol{z})|^2}{B_k(\boldsymbol{z})}. \tag{21}$$

By introducing auxiliary variables $\boldsymbol{\beta} = [\beta_1, ..., \beta_K]^T$, we reformulate the optimization problem as follows:

$$\max_{\boldsymbol{z}, \boldsymbol{\beta}} \sum_{k=1}^{K} \left(2Re\{\beta_k^* A_k(\boldsymbol{z})\} - |\beta_k|^2 B_k(\boldsymbol{z}) \right). \tag{22}$$

It is evident that the problem (21) is equivalent to the problem (22), which is verified by substituting $\beta_k = \frac{A_k(\boldsymbol{z})}{B_k(\boldsymbol{z})}$ into the optimization problem (22). Based on the above observations, we introduce closed-form FP scheme by dropping the quadratic transform in (22) to solve the optimization problem (17) as follows

$$\mathcal{P}(A2) \quad \max_{\boldsymbol{\alpha}, \boldsymbol{\beta}, \boldsymbol{o}_{RIS}, \boldsymbol{\theta}_g, \boldsymbol{W}, \boldsymbol{h}_{e,k}} f_{A2}(\boldsymbol{\alpha}, \boldsymbol{\beta}, \boldsymbol{o}_{RIS}, \boldsymbol{\theta}_g, \boldsymbol{W}, \boldsymbol{\zeta}), \tag{23a}$$

$$s.t. \ (17b), (17c), (20b), \tag{23b}$$

where the corresponding objective function is given by

$$\begin{aligned} f_{A2}(\boldsymbol{\alpha}, \boldsymbol{\beta}, \boldsymbol{o}_{RIS}, \boldsymbol{\theta}_g, \boldsymbol{W}, \boldsymbol{\zeta}) &= \sum_{k=1}^{K} \omega_k \left(\log(1+\alpha_k) - \alpha_k \right) \\ &+ \sum_{k=1}^{K} 2\sqrt{\omega_k(1+\alpha_k)} Re\left\{ \beta_k^* \sqrt{1-\zeta_k} \boldsymbol{h}_k^H \boldsymbol{w}_k \right\} \\ &- \sum_{k=1}^{K} |\beta_k|^2 \Big(\sum_{i=1}^{K} \left| \sqrt{1-\zeta_k} \boldsymbol{h}_k^H \boldsymbol{w}_i \right|^2 + \left| \sqrt{\zeta_k} \boldsymbol{h}_{e,k}^H \boldsymbol{w}_k \right|^2 + \sigma^2 \Big). \end{aligned} \tag{24}$$

Although we have transformed problem (17) into problem (24), it is still not straightforward to solve the problem $\mathcal{P}(A2)$ by simultaneously optimizing all variables. To mitigate this impact, we focus on optimizing the variables in an alternative manner. It is a remarkable fact that the computation cost of problem $\mathcal{P}(A2)$ increases with the increasing of the number of phase shifts. In addition, the CSI error optimization subproblem can be independently exploited to obtain the feasible solution. Motivated by this, we decouple it into four subproblems to deal with the transmit beamforming, RIS placement, phase shifts of RIS and CSI error in the following.

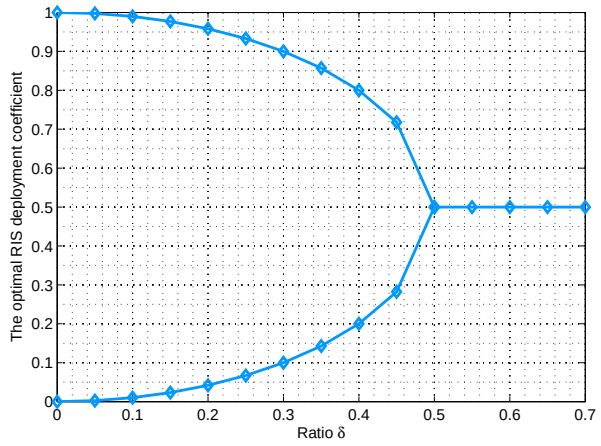

Fig. 3. The optimal RIS deployment coefficient $\xi^*(\delta)$ against distance-versus-altitude ratio δ.

A. Location Planning Optimization

We investigate the location planning with fixed the $\boldsymbol{\alpha}, \boldsymbol{\beta}, \boldsymbol{\theta}_g, \boldsymbol{W}$ and $\boldsymbol{\zeta}$. Since RIS is an integrated reflection surface, which is constituted by G RIS unit. Therefore, we just to estimate the position of the first RIS unit, e.g., $g = 1$. By that analogy, the position of the other RIS unit can be obtained. It is widely believed that RIS is considered to control and adjust the propagation direction, the direct channel from BS to UE is obstructed or can be estimated by closing the RIS. Therefore, the direct channel from BS to UE is not considered for the location planning optimization problem $\mathcal{P}(A2)$ in (23), which can be recast as

$$\min_{\boldsymbol{o}_{RIS_g}} \sum_{k=1}^{K} \frac{(H_{RIS_g}^2 + \|\boldsymbol{o}_{RIS_g} - \boldsymbol{o}_{UE_k}\|_2^2)\left((H_{BS} - H_{RIS_g})^2 + \|\boldsymbol{o}_{RIS_g} - \boldsymbol{o}_{BS}\|_2^2\right)}{\boldsymbol{A}_k + \boldsymbol{B}_k} \tag{25}$$

where

$$\boldsymbol{A}_k = 2\sqrt{\omega_k(1+\alpha_k)}Re\left\{\beta_k^*\sqrt{1-\zeta_k}(\boldsymbol{\theta}_g^H \mathrm{diag}(\boldsymbol{h}_{g,k}^H)\boldsymbol{V}_g)\boldsymbol{w}_k\right\},$$

$$\boldsymbol{B}_k = -|\beta_k|^2\Big(\sum_{i\neq k}^{K}\left|\sqrt{1-\zeta_k}(\boldsymbol{\theta}_g^H \mathrm{diag}(\boldsymbol{h}_{g,k}^H)\boldsymbol{V}_g)\boldsymbol{w}_i\right|^2\Big).$$

It can be observed that the optimization problem (25) is intrinsically a classical fractional programming problem, which can be solved by checking the first-order derivative of the location $\boldsymbol{o}_{RIS_g}$. As described above, the location of the coverage area satisfies $(o_o(1) - o_{UE}(1))^2 + (o_o(2) - o_{UE}(2))^2 \leq r^2$ and r denotes the radius of the coverage area. The center location of the coverage area $\boldsymbol{o}_o$ is used in place of $\boldsymbol{o}_{UE}$. After dropping irrelevant constant terms, the optimal horizontal placement of the RIS is given by

$$\boldsymbol{o}_{RIS_g} = \xi^*(\delta)\boldsymbol{o}_o \tag{26}$$

with

$$\xi^*(\delta) = \begin{cases} \dfrac{1}{2}, & \delta \geq \dfrac{1}{2} \\ \dfrac{1}{2} - \sqrt{\dfrac{1}{4} - \delta^2} \text{ or } \dfrac{1}{2} + \sqrt{\dfrac{1}{4} - \delta^2}, & \text{otherwise} \end{cases} \tag{27}$$

where $\xi^*(\delta)$ is called the ratio coefficient and $\delta = \frac{H_{RIS_g}}{D}$ and D is source-destination distance.

It is observed from (26) that the optimal horizontal placement of RIS only relies on $\delta = \frac{H_{RIS_g}}{D}$. As shown in Fig. 3, if the ratio coefficient $\delta \geq \frac{1}{2}$, the RIS should be placed at the central area between the source and destination. If the ratio coefficient $0 \leq \delta < \frac{1}{2}$, there exist two optimal placement locations for the RIS that are symmetrical about the midpoint.

B. Transmit Beamforming Optimization

One may focus on the variables $\boldsymbol{w}_k$ by fixing the remaining variables. Let $\boldsymbol{W} = \{\boldsymbol{w}_1, \boldsymbol{w}_2, ..., \boldsymbol{w}_K\}$, the optimization problem (23) with respect to the $\boldsymbol{W}$ is optimized through the following problem

$$\mathcal{P}(A3) \quad \max_{\boldsymbol{\alpha},\boldsymbol{\beta},\boldsymbol{w}_k} f_{A3}(\boldsymbol{w}_k, \boldsymbol{\alpha}, \boldsymbol{\beta}), \tag{28a}$$

$$s.t.\ \mathrm{tr}\left(\boldsymbol{W}^H\boldsymbol{W}\right) \leq P_{\max}, \tag{28b}$$

where $\boldsymbol{\beta} = [\beta_1, ..., \beta_K]^T$ is the auxiliary vector.

By dropping irrelevant constant terms, the objective function in (28a) can be rewritten as

$$f_{A3}(\boldsymbol{w}_k, \boldsymbol{\alpha}, \boldsymbol{\beta}) = \sum_{k=1}^{K} 2\sqrt{\omega_k(1+\alpha_k)}Re\left\{\beta_k\sqrt{1-\zeta_k}\boldsymbol{h}_k^H\boldsymbol{w}_k\right\} - \sum_{k=1}^{K}|\beta_k|^2\Big(\sum_{i=1}^{K}\left|\sqrt{1-\zeta_k}\boldsymbol{h}_k^H\boldsymbol{w}_i\right|^2 + \left|\sqrt{\zeta_k}\boldsymbol{h}_{e,k}^H\boldsymbol{w}_k\right|^2 + \sigma^2\Big). \tag{29}$$

It is worth mentioning that the optimization problem (28) includes the variables $\boldsymbol{\alpha}$, $\boldsymbol{\beta}$ and $\boldsymbol{w}_k$. To solve this problem, we decompose the optimization variables $\boldsymbol{\alpha}$, $\boldsymbol{\beta}$ and $\mathbf{w}_k$ by exploiting the Lagrangian multiplier method, which can be expressed as

$$\mathcal{L}_k(\boldsymbol{w}_k, \boldsymbol{\alpha}, \boldsymbol{\beta}) = 2\sqrt{\omega_k(1+\alpha_k)}Re\left\{\beta_k^*\sqrt{1-\zeta_k}\boldsymbol{h}_k^H\boldsymbol{w}_k\right\} - |\beta_k|^2\Big(\sum_{i=1}^{K}|\sqrt{1-\zeta_k}\boldsymbol{h}_k^H\boldsymbol{w}_i|^2 + \left|\sqrt{\zeta_k}\boldsymbol{h}_{e,k}^H\boldsymbol{w}_k\right|^2 + \sigma^2\Big) + \eta\left(\mathrm{tr}(\boldsymbol{W}^H\boldsymbol{W}) - P_{\max}\right), \tag{30}$$

where $\eta \geq 0$ is the Lagrange multiplier corresponding to the transmit power constraint (30).

Thus, the optimal transmit beamforming vector $\boldsymbol{w}_k$ is updated by directly the use of the Karush-Kuhn-Tucker (KKT) optimality condition as follows

$$\boldsymbol{w}_k = \sqrt{\omega_k(1+\alpha_k)}\beta_k\sqrt{1-\zeta_k}\big(\eta\boldsymbol{I}_N + |\beta_k|^2 \times \big(\sum_{i=1}^{K}(1-\zeta_k)\boldsymbol{h}_k\boldsymbol{h}_k^H + \zeta_k\boldsymbol{h}_{e,k}\boldsymbol{h}_{e,k}^H\big)\big)^{-1}\boldsymbol{h}_k. \tag{31}$$

Let $\mathbf{X} = \sum_{i=1}^{K}(1-\zeta_k)\boldsymbol{h}_k\boldsymbol{h}_k^H + \zeta_k\boldsymbol{h}_{e,k}\boldsymbol{h}_{e,k}^H$ and $\boldsymbol{g}_k = \sqrt{\omega_k(1+\alpha_k)(1-\zeta_k)}\beta_k\boldsymbol{h}_k$, the equation (31) can be rewritten as

$$\left(\eta\boldsymbol{I}_N + \beta_k^2\mathbf{X}\right)^{-1}\boldsymbol{g}_k = \boldsymbol{w}_k. \tag{32}$$

Thus, the derivation of the Lagrange multiplier η is

$$\begin{aligned}\frac{\partial \mathrm{tr}(\boldsymbol{w}_k\boldsymbol{w}_k^H)}{\partial \eta} &= \mathrm{tr}\left(\left(\frac{\partial \mathrm{tr}(\boldsymbol{w}_k\boldsymbol{w}_k^H)}{\partial \boldsymbol{w}_k}\right)^H \frac{\partial \boldsymbol{w}_k}{\partial \eta}\right) \\ &= -2\mathrm{tr}\left(\boldsymbol{w}_k^H\left(\eta\boldsymbol{I}_N+\beta_k^2\mathbf{X}\right)^{-1}\left(\eta\boldsymbol{I}_N+\beta_k^2\mathbf{X}\right)^{-1}\boldsymbol{g}_k\right) \\ &= -2\mathrm{tr}\left(\boldsymbol{w}_k^H(\eta\boldsymbol{I}_N+\beta_k^2\mathbf{X})^{-1}\boldsymbol{w}_k\right),\end{aligned} \tag{33}$$

which shows that (31) is monotonically decreased with the increasing η. Accordingly, the optimal η is determined by minimizing the η with the constraint (28b). That is

$$\eta = \left\{\eta \geq 0 : \mathrm{tr}\big(\boldsymbol{W}^H\boldsymbol{W}\big) = P_{\max}\right\}. \tag{34}$$

By setting $\partial f_{A3}(\boldsymbol{W},\beta_k)/\partial\beta_k = 0$, the optimal β_k is given by

$$\beta_k = \frac{\sqrt{\omega_k(1+\alpha_k)(1-\zeta_k)}\boldsymbol{h}_k^H\boldsymbol{w}_k}{\sum_{i=1}^K(1-\zeta_k)|\boldsymbol{h}_k^H\boldsymbol{w}_i|^2+\zeta_k\left|\boldsymbol{f}_k^H\boldsymbol{h}_{e,k}^H\boldsymbol{w}_k\right|^2+\sigma^2}. \tag{35}$$

Similarity, the optimal α_k is given by

$$\alpha_k = \frac{\chi_k^2+\chi_k\sqrt{\chi_k^2+4}}{2}, \tag{36}$$

where $\chi_k = \frac{1}{\sqrt{\omega_k}}Re\big\{\sqrt{1-\zeta_k}\beta_k^*\boldsymbol{h}_k^H\boldsymbol{w}_k\big\}$.

C. Phase Shifts Optimization

After the completion of transmit beamforming at the BS, it needs to further solve the phase shifts optimization problem by adjusting PSs pertaining to the RIS. With mathematical manipulations, the optimal solution to the problem (23) with respect to $\boldsymbol{\theta}_g$ can be rewritten as

$$\mathcal{P}(A4) \quad \max_{\boldsymbol{\theta}_g}\Big\{f_{\mathcal{A}4}(\boldsymbol{\theta}_g) \triangleq \sum_{g=1}^{G}\left(\boldsymbol{\theta}_g^H\boldsymbol{Q}\boldsymbol{\theta}_g - 2Re\{\boldsymbol{\theta}_g^H\boldsymbol{c}\}\right)\Big\}, \tag{37a}$$

$$s.t.\ \ \theta_{g,m}\in\mathcal{F}_c, \quad c=\{1,2,3\}, \tag{37b}$$

where $\boldsymbol{Q}$ and $\boldsymbol{c}$ are respectively given by

$$\boldsymbol{Q} = \sum_{k=1}^K(1-\zeta_k)|\beta_k|^2\sum_{i=1}^K\boldsymbol{H}_{g,k}\boldsymbol{w}_k\boldsymbol{w}_k^H\boldsymbol{H}_{g,k}^H,$$

$$\boldsymbol{c} = \sum_{k=1}^K\left(\sqrt{\omega_k(1+\alpha_k)(1-\zeta_k)}\beta^*\left(\boldsymbol{H}_{g,k}\boldsymbol{w}_k\right)\right).$$

However, the major challenge of problem (37) arises from the non-convexity of the phase shifts constraints in (37b). The gradient descent scheme provides excellent spectral efficiency to deal with the constrained optimization problem [44]. However, this approach *cannot* guarantee that the solution of problem (37) is feasible due to the phase shifts constraint. To tackle the above challenge, the gradient projection (GP) framework is developed, which projects the feasible solution obtained by the gradient descent approach onto the constraint set $\mathcal{F}_c$. More specifically, the GP framework is updated in each iteration, which is given by

$$\tilde{\boldsymbol{\theta}}_g^{(t+1)} = \boldsymbol{\theta}_g^{(t)} - \mu\nabla f_{\mathcal{A}4}(\boldsymbol{\theta}_g^{(t)}) \tag{38a}$$

$$\boldsymbol{\theta}_g^{(t+1)} = \arg\min_{\boldsymbol{\theta}_g\in\mathcal{F}_c}\left\|\tilde{\boldsymbol{\theta}}_g^{(t+1)}-\boldsymbol{\theta}_g\right\|_2^2 \tag{38b}$$

where μ denotes a pre-specified stepsize and $\nabla f_{\mathcal{A}4}(\boldsymbol{\theta}_g) = -(\boldsymbol{Q}^H+\boldsymbol{Q})\boldsymbol{\theta}_g^{(t)}+2\boldsymbol{c}^H$ denotes the gradient of the objective function (37a). $\boldsymbol{\theta}_g^{(t+1)}$ is the result of gradient projection, which is the closest feasible vector to $\tilde{\boldsymbol{\theta}}_g^{(t+1)}$ based on Euclidean distance. Equation (38b) means that the calculated phase shifts in each step of the gradient ascent of (38a) should be projected onto the constraint set $\mathcal{F}_c$, which is the feasible region of (4). The stopping criteria is provided as follows

$$\left|\frac{f_{\mathcal{A}4}\left(\boldsymbol{\theta}_g^{(t+1)}\right)-f_{\mathcal{A}4}\left(\boldsymbol{\theta}_g^{(t)}\right)}{f_{\mathcal{A}4}\left(\boldsymbol{\theta}_g^{(t)}\right)}\right| \leq \varepsilon,$$

where ε is the stopping condition.

It is worth that the GP framework is introduced to achieve the feasible solution of phase shifts optimization problem, but such a projection operator may cause high control overhead and slow convergence problem. To further explain the convergence for GP framework, the following proposition is stated by carefully choosing the step size.

Proposition I. Let $\boldsymbol{\theta}_g^{(t)}$ be the sequence of feasible solutions obtained by the GP scheme. If λ_{max} is the maximum eigenvalue of $\{\boldsymbol{Q}\}$ that satisfying $\mu \leq \frac{1}{4\lambda_{\max}}$, then we have $f(\boldsymbol{\theta}_g^{(t+1)}) \leq f(\boldsymbol{\theta}_g^{(t)})$.

Proof: See Appendix A. ■

D. CSI Error Optimization

As shown in the optimization problem (23), the CSI error $\boldsymbol{h}_{e,k}$ are inevitable due to unsuspected feedback delay, the residual CSI error will substantially impact the overall system performance due to imperfect CSI. Especially, many other factors in the environment can affect CSI performance, including block the line of sight, factors of time-attenuation and path-attenuation. To solve low channel utilization problem caused by time-delay channel in wireless networks, it is necessary to suppress the CSI error $\boldsymbol{h}_{e,k}$. From (12), it is observed that the CSI error $\boldsymbol{h}_{e,k}$ is related to ζ_k. Therefore, we focus on optimizing the variable ζ_k in the CSI error optimization problem. Then, the optimization problem (23) with respect to ζ_k is transformed to

$$\mathcal{P}(A5) \quad \min_{\zeta_k} f_{A5}(\zeta_k), \tag{39}$$

where the objective function is

$$\begin{aligned}f_{A5}(\zeta_k) = &\sum_{k=1}^K 2\sqrt{\omega_k(1+\alpha_k)}Re\Big\{\beta_k\sqrt{1-\zeta_k}\boldsymbol{h}_k^H\boldsymbol{w}_k\Big\} \\ &-\sum_{k=1}^K|\beta_k|^2\Big(\sum_{i=1}^K\left|\sqrt{1-\zeta_k}\boldsymbol{h}_k^H\boldsymbol{w}_i\right|^2+\left|\sqrt{\zeta_k}\boldsymbol{h}_{e,k}^H\boldsymbol{w}_k\right|^2+\sigma^2\Big)\end{aligned} \tag{40}$$

It seems obvious that the optimization problem (39) is difficult to obtain an optimal solution ζ_k, since adjusting the priority ω_k and the error factor ζ_k will also affect the performance of transmit beamforming in (31) and the performance of phase shifts in (38). To tackle this issue, the problem (39) with respect to the error factor ζ_k is transformed as a MOEA/D-based multiobjective optimization problem, which can be reformulated as

$$\min F_{A5} = \{g_1(\boldsymbol{\zeta}), g_2(\boldsymbol{\omega}), g_3(\boldsymbol{h}_{e,k})\}, \tag{41}$$

where

$$\begin{aligned} g_1(\boldsymbol{\zeta}) &= \sum_{k=1}^{K} Re\Big\{\beta_k^* \sqrt{1-\zeta_k}\boldsymbol{h}_k^H \boldsymbol{w}_k\Big\} \\ &\quad - \sum_{k=1}^{K} |\beta_k|^2 \Big(\sum_{i=1}^{K} \Big|\sqrt{1-\zeta_k}\boldsymbol{h}_k^H \boldsymbol{w}_i\Big|^2 + \Big|\sqrt{\zeta_k}\boldsymbol{h}_{e,k}^H \boldsymbol{w}_k\Big|^2 \Big), \\ g_2(\boldsymbol{\omega}) &= \frac{1}{|\boldsymbol{\omega}|}, \quad \boldsymbol{\omega} = [\omega_1, ..., \omega_K]^T, \\ g_3(\mathbf{E}(\nu_t, \nu_r)) &= \frac{1}{|\mathbf{E}(\nu_t, \nu_r)|}. \end{aligned} \tag{42}$$

and $\mathbf{E}(\nu_t, \nu_r)$ is the beamforming gain. It is observed in [45] that $|\boldsymbol{h}_k^H \boldsymbol{w}_k|$ increases with the increasing of the beamforming gain $|\mathbf{E}(\nu_t, \nu_r)|$.

Next, the MOEA/D with Tchebycheff approach [46] is exploited to solve the problem (41). The main idea is to divided the optimization problem (41) into a series of scalar optimization problems. Thus, all of the subproblems can be optimized simultaneously to approximate the Pareto front (PF). Specifically, in preliminary stages, the Euclidean distance is considered to compute T_c nearest neighbors of the weight vectors $\boldsymbol{u}^i$ for each $i \in \{1, \cdots, N_{pop}\}$, and generate the set $\Omega(i)$, whose indexes are contained in $\Omega(i) = \{i_1, i_2, ..., i_{T_c}\}$. For each subproblems, we generate the decision variables $\{\varpi_k^1, \varpi_k^2, ..., \varpi_k^{pop}\}$ randomly, and set $FV_i = J(\varpi_k)$. Let $\varrho_j = \min\{F_{A5}\}$ be the best-so-far solution of the problem (41). For each $i = 1, ..., N_{pop}$, we randomly select two indexes l_1, l_2 from $\Omega(i)$, and then generate a decision variable ϖ_k^c from $\varpi_k^{l_1}$ and $\varpi_k^{l_2}$ by differential evolution (DE) [46]. Subsequently, we update the population by comparing best-so-far solutions and current solutions as follows:

If $\varrho_j > f_j(\varpi_k^c)$, for each $j = 1, \cdots, d$, the best-so-far solution ϱ_j is updated. Then, for each $j \in \Omega(i)$, if $J\left(\varpi_k^c \mid \boldsymbol{u}^j, \boldsymbol{\varrho}\right) \leq J\left(\varpi_k^j \mid \boldsymbol{u}^j, \boldsymbol{\varrho}\right)$, we replace the decision variable ϖ_k^j and F-value FV_j by ϖ_k^c and $J(\varpi_k^c)$, respectively, where $J\left(\varpi_k^c \mid \boldsymbol{u}^j, \boldsymbol{\varrho}\right) = \max_{1 \leq t \leq d}\left\{\boldsymbol{u}_t^j \, |g_t(\varpi_k^c) - \varrho_t|\right\}$. If the condition is satisfied, iteration stop and output EP. Otherwise, go to the step update. Finally, the optimal solution is determined on the PF for the three fitness functions.

As above mentioned, variables $(\boldsymbol{\alpha}^{(0)}, \boldsymbol{\beta}^{(0)}, \boldsymbol{o}_{RIS}^{(0)}, \boldsymbol{\theta}_g^{(0)}, \boldsymbol{W}^{(0)}, \boldsymbol{\zeta}^{(0)})$ are initialized at the beginning of iteration, these variables are updated at the end of each iteration, and repeat this process until convergence. The proposed iterative algorithm is outlined in Algorithm 1. Based on $\mathcal{P}(A1)$ and $\mathcal{P}(A4)$, the overall complexity of the above algorithm can be given by $\mathcal{O}(M^3 + MN^2 + K(2M^3 + MN^2) + IG(M + NM^2 + MN) + KMN)$, where the complexity of optimizing the phase shifts is significantly reduced, due to the separate design.

Algorithm 1 The GP-MEA for Solving the problem (23)

1: **Initialization**: $t = 0$, set P^t and the stopping criterion.
2: **Input**: $\boldsymbol{y}$, $\boldsymbol{H}_{g,k}$, $\boldsymbol{h}_{d,k}$
3: **repeat**
4: ***Location Planning Optimization***: Update $\boldsymbol{o}_{RIS}$ by solving the problem (25).
5: ***Transmit Beamforming Optimization***: Update variables $\boldsymbol{W}$ by solving the problem (28);
6: Obtain the optimal $\boldsymbol{w}_k$, α_k and β_k by (34)-(36);
7: ***Passive Beamforming Optimization***: Update variable $\boldsymbol{\theta}_g$ by solving the problem (37);
8: ***Estimation Error Optimization***: Update the variable $\boldsymbol{\zeta}$ by solving the problem (41);
9: **End**
10: **until** The obtained solution is feasible;
11: **Output**: $\{\boldsymbol{o}_{RIS}, \boldsymbol{\theta}_g, \boldsymbol{W}, \boldsymbol{\zeta}, \boldsymbol{\alpha}, \boldsymbol{\beta}\}$

V. Simulation Results

This section presents numerical simulation results to validate the effectiveness of the RIS-assisted beamforming scheme with imperfect CSIs. To provide comparisons, we assume that the RIS with 64 reflecting elements is located to serve the UEs that suffer from severe signal attenuation/interruption in the BS-user direct link. Let's suppose that the BS is located at (0, 0) with 16 antennas. According to [47] and [48], we define the channel gain as $g_v \sim \mathcal{CN}(0, 10^{-0.1\mathcal{Y}(r)})$, where $\mathcal{Y}(r) = \ddot{\varrho}_a + 10\ddot{\varrho}_b \lg(r) + \xi$ with $\mathcal{N}(0, \sigma^2)$ and r is the distance between BS and UE. The values of $\ddot{\varrho}_a$ and $\ddot{\varrho}_b$ is derived from Friis' law. Each RIS unit size is set as $M_{az} = 10$ and $M_{el} = 2$, which is used to provide high-quality yet efficient link from the BS to UEs. We assume that $G = 2$ RIS units located at (50 m, 30 m). Unless otherwise stated, the pathloss is set according to the 3GPP propagation environment [49]. In particular, the total transmit power is set to $P_{\max} = 30$ dBm.

A. Convergence Performance

The convergence of the proposed GP-MEA are investigated in Fig. 4, where the spectral efficiency is shown versus the number of iterations. It is found that under our theoretical characterization of beamforming algorithm, the curves gradually increase and exhibit trend of convergence after about 6 iterations. This indicates that the proposed algorithm is convergence. It should be noted that as the number of phase shifts M increases, this involves complex solutions for the four subproblems of the proposed algorithm, which leads to more computation time for each iteration, and hence the total computation time by the GP-MEA still increases even with fewer iterations.

Accordingly, the non-dominated set of the above four CSI error achieved by the mmultiobjective optimization scheme is shown in Fig. 5. It can be seen that most of the non-dominated

This article has been accepted for publication in IEEE Transactions on Wireless Communications. This is the author's version which has not been fully edited and content may change prior to final publication. Citation information: DOI 10.1109/TWC.2022.3222218

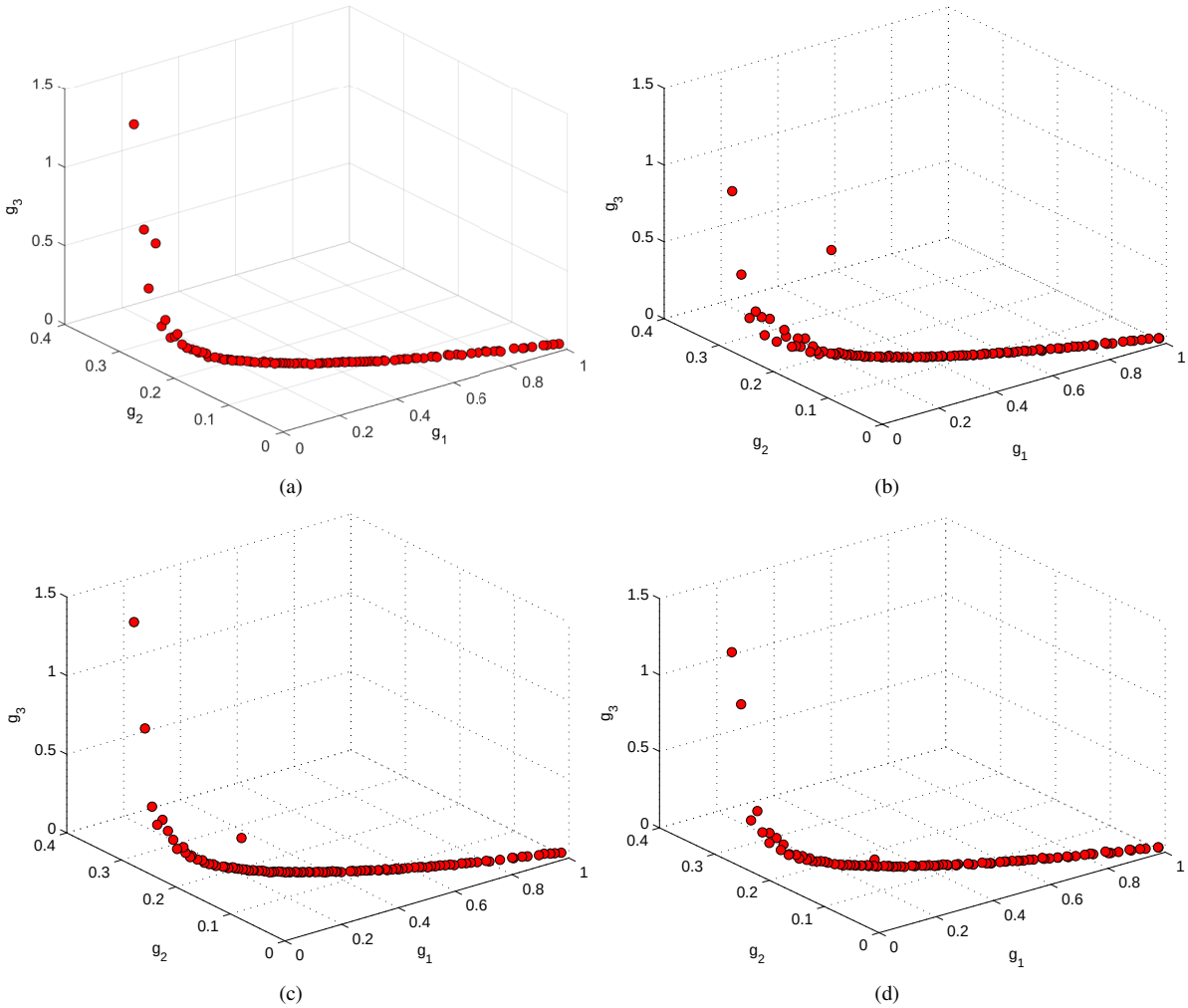

Fig. 5. The convergence behavior of multiobjective optimization scheme with MOEA/D.

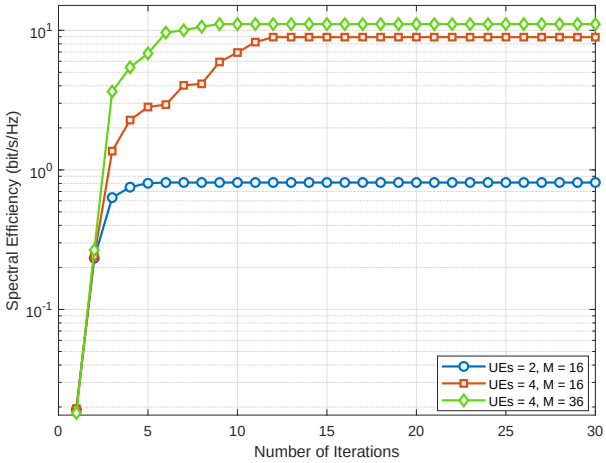

Fig. 4. Convergence behavior of the proposed GP-MEA.

solutions of each CSI error result lie on a real Pareto front, due to the fact that the generated non-dominated solution set is better than the previous solution at current iteration, and thereby the algorithm can obtain the optimal solutions that is close to the Pareto-optimal solution. Moreover, it can be seen that there is a trade-off between the decoder, gain factor and estimation error. Furthermore, the beam gain performance is depicted in Fig. 6. We can observe that the proposed scheme is superior to conventional schemes, such as without phase shifts optimization.

B. Impact of the transmit power

To study an overall observation of the performance of the proposed GP-MEA, we investigated the spectral efficiency versus the transmit power for $M = 25$ and $K = 4$. As illustrated in Fig. 7, the spectral efficiency of all considered schemes increase with the transmit power $P_{\max}$ increasing. It is observed that the proposed scheme with phase shifts set $\mathcal{F}_2$ consume less transmit power than the "Random phase shifts" scheme, since the RIS phase shifts are not optimized. Furthermore, it is also observed that a higher transmit power leads to a higher spectral efficiency. From Fig. 8, we investigated the the spectral efficiency achieved by different schemes versus the number of UEs for the number of phase shifts $M = 25$, where three types of phase shifts set are considered in this case. It is observed that the phase shifts set has a great influence on the improvement of system performance with the number of

This article has been accepted for publication in IEEE Transactions on Wireless Communications. This is the author's version which has not been fully edited and content may change prior to final publication. Citation information: DOI 10.1109/TWC.2022.3222218

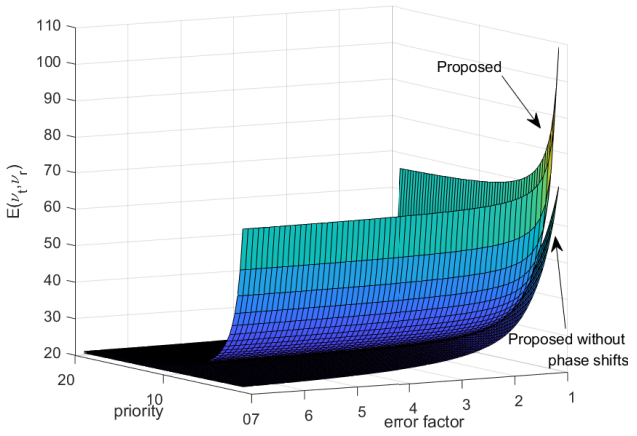

Fig. 6. Tradeoff CSI error, beamforming gain and error factor between proposed and conventional scheme.

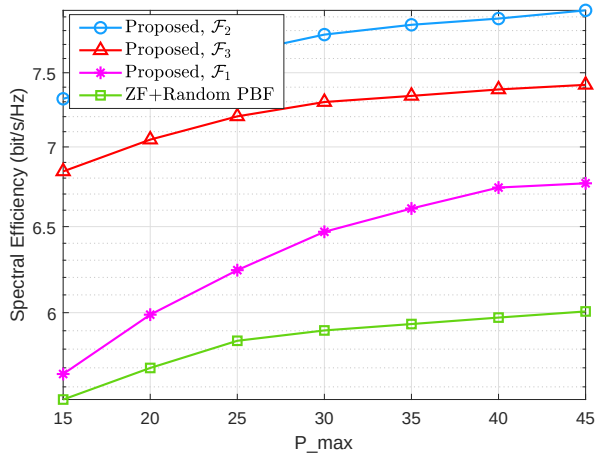

Fig. 7. Spectral efficiency versus the transmit power $P_{\max}$ for multi-RIS assisted system when M = 25, $K = 2$.

UEs K increasing. For achieving the same spectral efficiency, the proposed scheme with phase shifts set $\mathcal{F}_2$ outperforms the phase shifts cases $\mathcal{F}_1$ and $\mathcal{F}_3$, which also means that the proposed scheme is effective. This is because more RIS reflecting elements bring more reflection paths by optimizing phase shifts, which improves the performance of system.

C. Effect of RIS Deployment

By moving the RIS from (10 m, 30 m) to (110 m, 30 m), the effects of RIS deployment position is investigated in this subsection. For the sake of presentation, the phase shifts set are given by $\{\mathcal{F}_c|c = 1, 2, 3\}$. Fig. 9 shows the spectral efficiency of different schemes with respect to the horizontal distance of the RIS. As expected, increasing horizontal coordinate x from 10 m to 110 m leads to the spectral efficiency decreasing, which means long-distance information transmission results in high propagation path loss. According to Fig. 9, different phase shifts sets may lead to different system performance. We observe that the performance of the proposed GP-MEA with optimized phase shifters still better than the phase shifters schemes $\mathcal{F}_1$ and $\mathcal{F}_3$ regardless of the RIS deployment.

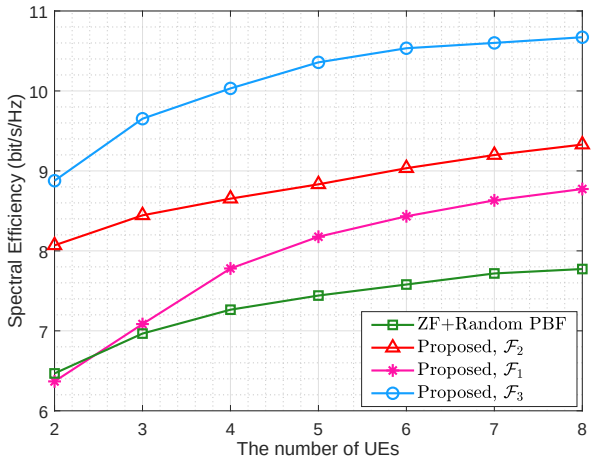

Fig. 8. Spectral efficiency versus the number of the UEs for multi-RIS assisted system when M = 25.

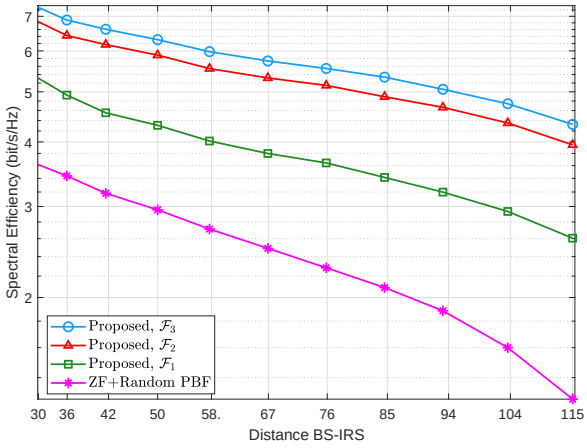

Fig. 9. Spectral efficiency versus the distance between BS and RIS for multi-RIS assisted system when M = 25.

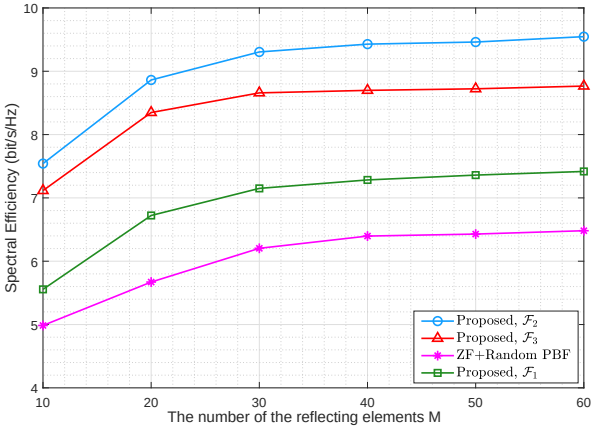

Fig. 10. The spectral efficiency versus the number of the reflecting elements for multi-RIS assisted system with $N = 64$.

D. Effect of RIS size

Fig. 10 displays the SE versus the number of phase shifters M of RIS size. From a detailed inspection, the SE monotonically increases as the number of reflecting elements increasing,

when multi-units is used to RIS. This is because large number of reflecting elements of RISs introduce additional reflecting paths, which results in high SE of the system. As shown in Fig. 10, the SE of all schemes increases with the number of phase shifts M increasing. As predicted by the previous analysis, although increasing the number of phase shifts M consumes more power, the SE of the proposed GP-MEA is still better than that of the schemes with $\mathcal{F}_1$ and $\mathcal{F}_3$, when optimal PSs are used to the RIS. Comparing between the three type PSs set, it is seen that the proposed GP-MEA is not highly sensitive to the number of RIS units, when the number of of reflecting elements larger than 30.

VI. Conclusion

In this paper, we proposed a robust beamforming scheme, which strikes a balance between the beamforming gain and the CSI error, and the importance of exploiting both the passive beamforming of RIS and flexible deployment in designing multi-RIS assisted wireless communications. We formulated a WSM problem that maximizes the beamforming gain and minimizes the channel CSI error at the same time. The closed-form FP method was employed to make the non-convex WSM problem for the beamforming tractable. Furthermore, to alleviate the effects of the CSI error and RIS placement, the joint optimization of transmit/reflect beamforming, CSI error and RIS placement algorithm was designed to overcome the channel uncertainty. Simulation results demonstrated that the developed approach can achieve significant SE compared to several benchmark schemes, providing a possibility for robust beamforming design with imperfect CSI in practical RIS-assisted systems.

Appendix A
Proposition I

Proof: According to the problem (37), the gradient of the objective function can be computed as $f_{_{\mathcal{A}4}}(\boldsymbol{\theta}) \triangleq -2(\boldsymbol{c}-\boldsymbol{Q}\boldsymbol{\theta})$. Accordingly, we have

$$\begin{aligned}\|\nabla f(\boldsymbol{\theta}) - \nabla f(\boldsymbol{y})\|_2^2 &= \|2\boldsymbol{Q}(\boldsymbol{\theta}-\boldsymbol{y})\|_2^2 \\ &\overset{(a)}{\leq} 4\|\boldsymbol{Q}\|_2^2\|(\boldsymbol{\theta}-\boldsymbol{y})\|_2^2 \\ &\overset{(b)}{=} \frac{1}{\mu}\|(\boldsymbol{\theta}-\boldsymbol{y})\|_2^2\end{aligned} \tag{43}$$

where (a) is from $\|2\boldsymbol{Q}(\boldsymbol{\theta}-\boldsymbol{y})\|_2^2 \leq 4\|\boldsymbol{Q}\|_2^2\|(\boldsymbol{\theta}-\boldsymbol{y})\|_2^2$, (b) follows the fact that the stepsize is given by satisfying $\mu \in (0, 4\lambda_{\max}(\boldsymbol{Q}^T\boldsymbol{Q})]$. $\nabla f(\boldsymbol{\theta})$ is Lipschitz continuous gradient with the corresponding parameter $\frac{1}{\mu}$, and thus we obtain the following relation:

$$f(\boldsymbol{\theta}) = \underbrace{f(\boldsymbol{y}) + \nabla f(\boldsymbol{y})^H(\boldsymbol{\theta}-\boldsymbol{y}) + \frac{1}{2\mu}\|(\boldsymbol{\theta}-\boldsymbol{y})\|_2^2}_{g(\boldsymbol{\theta},\boldsymbol{y})} \tag{44}$$

where $g(\boldsymbol{\theta},\boldsymbol{y})$ denotes the quadratic upper bound of the surrogate function $f(\boldsymbol{\theta})$. Considering the equality of (44) holds if and only if $\boldsymbol{\theta} = \boldsymbol{y}$, $\boldsymbol{y}$ is adopted instead of $\boldsymbol{\theta}^{(t)}$ that satisfying $\boldsymbol{\theta}^{(t)} = \boldsymbol{y}^{(t)}$. Inspired by [50], the iterative algorithm with majorization-minimization is exploited to solve problem (37). At each iteration t of the majorization-minimization framework, $\boldsymbol{y}^{(t)}$ is updated by minimizing the difference of the current point $\boldsymbol{\theta}^{(t)}$ between the surrogate function and the objective function. Thus, we have $f(\boldsymbol{\theta}) = g(\boldsymbol{\theta},\boldsymbol{y})$. Furthermore, according to the MM framework, the surrogate function with respect to $\boldsymbol{\theta}$ is updated by fixing $\boldsymbol{\theta} = \boldsymbol{y}$, i.e.,

$$\begin{aligned}\boldsymbol{\theta}^{(t+1)} &= \arg\min g(\boldsymbol{\theta},\boldsymbol{\theta}^{(t)}) \\ &= \arg\min \boldsymbol{\theta}^H\nabla f(\boldsymbol{\theta}^{(t)}) + \frac{1}{2\mu}\|\boldsymbol{\theta}\|_2^2 - \frac{1}{\mu}\boldsymbol{\theta}^H\boldsymbol{\theta}^{(t)} \\ &= \arg\min \frac{1}{2\mu}\left\|\boldsymbol{\theta} - \left(\boldsymbol{\theta}^{(t)} - \mu\nabla f(\boldsymbol{\theta}^{(t)})\right)\right\|_2^2 \\ &\overset{(a)}{=} \arg\min \frac{1}{2\mu}\|\boldsymbol{\theta} - \mathcal{P}_{\mathcal{F}_c}(\tilde{\boldsymbol{\theta}}^{(t+1)})\|_2^2\end{aligned} \tag{45}$$

where (a) is from $\tilde{\boldsymbol{\theta}}^{(t+1)} = \boldsymbol{\theta}^{(t)} - \mu\nabla f(\boldsymbol{\theta}^{(t)})$, $\mathcal{P}_{\mathcal{F}_c}(\cdot)$ is the projection operator, which is the closest feasible vector to $\tilde{\boldsymbol{\theta}}^{(t+1)}$ based on Euclidean distance. It is defined as

$$\mathcal{P}_{\mathcal{F}_c}(\boldsymbol{\theta}_g^{(t+1)}) = \arg\min_{\boldsymbol{\theta}_g\in\mathcal{F}_c}\left\|\tilde{\boldsymbol{\theta}}_g^{(t+1)} - \boldsymbol{\theta}_g\right\|_2^2. \tag{46}$$

From the above, one can conclude that the sequence $\{f(\boldsymbol{\theta}^{(t)})\}$ generated by the GP method is non-increasing because of

$$f\left(\boldsymbol{\theta}^{(t+1)}\right) \overset{(a)}{\leq} f\left(\boldsymbol{\theta}^{(t+1)},\boldsymbol{y}^t\right) \overset{(b)}{\leq} f\left(\boldsymbol{\theta}^{(t)},\boldsymbol{y}^t\right) = f\left(\boldsymbol{\theta}^{(t)}\right) \tag{47}$$

where (a) follows from (44) and (b) is from the fact that (45). ■

References

[1] T. L. Marzetta, "Noncooperative cellular wireless with unlimited numbers of base station antennas," *IEEE Transactions on Wireless Communications*, vol. 9, no. 11, pp. 3590–3600, 2010.

[2] Z. Chen, J. Tang, N. Zhao, M. Liu, and D. K. C. So, "Hybrid beamforming with discrete phase shifts for ris-assisted multiuser SWIPT system," *IEEE Wireless Communications Letters*, pp. 1–6, 2022.

[3] Z. Chen, J. Tang, X. Y. Zhang, D. K. C. So, S. Jin, and K.-K. Wong, "Hybrid evolutionary-based sparse channel estimation for irs-assisted mmwave MIMO systems," *IEEE Transactions on Wireless Communications*, vol. 21, no. 3, pp. 1586–1601, 2022.

[4] W. Tang, M. Z. Chen, X. Chen, J. Y. Dai, Y. Han, M. Di Renzo, Y. Zeng, S. Jin, Q. Cheng, and T. J. Cui, "Wireless communications with reconfigurable intelligent surface: Path loss modeling and experimental measurement," *IEEE Transactions on Wireless Communications*, vol. 20, no. 1, pp. 421–439, 2021.

[5] Z. Chen, J. Tang, X. Y. Zhang, Q. Wu, Y. Wang, D. K. C. So, S. Jin, and K.-K. Wong, "Offset learning based channel estimation for intelligent reflecting surface-assisted indoor communication," *IEEE Journal of Selected Topics in Signal Processing*, vol. 16, no. 1, pp. 41–55, 2022.

[6] W. Yan, X. Yuan, Z. Q. He, and X. Kuai, "Passive beamforming and information transfer design for reconfigurable intelligent surfaces aided multiuser MIMO systems," *IEEE Journal on Selected Areas in Communications*, vol. 38, no. 8, pp. 1793–1808, 2020.

[7] Y. Cao, T. Lv, Z. Lin, and W. Ni, "Delay-constrained joint power control, user detection and passive beamforming in intelligent reflecting surface-assisted uplink mmwave system," *IEEE Transactions on Cognitive Communications and Networking*, vol. 7, no. 2, pp. 482–495, 2021.

[8] C. Wang, Z. Li, J. Shi, and D. W. K. Ng, "Intelligent reflecting surface-assisted multi-antenna covert communications: Joint active and passive beamforming optimization," *IEEE Transactions on Communications*, vol. 69, no. 6, pp. 3984–4000, 2021.

[9] Q. Wu and R. Zhang, "Beamforming optimization for wireless network aided by intelligent reflecting surface with discrete phase shifts," *IEEE Transactions on Communications*, vol. 68, no. 3, pp. 1838–1851, 2020.

[10] Z. Chen, J. Tang, H. tang, D. K. C. So, and K. Wong, "Channel estimation of IRS-aided communication systems with hybrid multi-objective optimization," in *Proc IEEE International Conference on Communications (ICC)*, pp. 1–6, 2021.

[11] Y. Han, W. Tang, S. Jin, C.-K. Wen, and X. Ma, "Large intelligent surface-assisted wireless communication exploiting statistical CSI," *IEEE Transactions on Vehicular Technology*, vol. 68, no. 8, pp. 8238–8242, 2019.

[12] Q. Wu and R. Zhang, "Intelligent reflecting surface enhanced wireless network via joint active and passive beamforming," *IEEE Transactions on Wireless Communications*, vol. 18, no. 11, pp. 5394–5409, 2019.

[13] Q. Wu and R. Zhang, "Intelligent reflecting surface enhanced wireless network: Joint active and passive beamforming design," in *2018 IEEE Global Communications Conference (GLOBECOM)*, pp. 1–6, 2018.

[14] P. Wang, J. Fang, X. Yuan, Z. Chen, and H. Li, "Intelligent reflecting surface-assisted millimeter wave communications: Joint active and passive precoding design," *IEEE Transactions on Vehicular Technology*, vol. 69, no. 12, pp. 14960–14973, 2020.

[15] C. Huang, A. Zappone, G. C. Alexandropoulos, M. Debbah, and C. Yuen, "Reconfigurable intelligent surfaces for energy efficiency in wireless communication," *IEEE Transactions on Wireless Communications*, vol. 18, no. 8, pp. 4157–4170, 2019.

[16] C. Huang, S. Hu, G. C. Alexandropoulos, A. Zappone, C. Yuen, R. Zhang, M. D. Renzo, and M. Debbah, "Holographic MIMO surfaces for 6G wireless networks: Opportunities, challenges, and trends," *IEEE Wireless Communications*, vol. 27, no. 5, pp. 118–125, 2020.

[17] S. Hong, C. Pan, H. Ren, K. Wang, and A. Nallanathan, "Artificial-noise-aided secure MIMO wireless communications via intelligent reflecting surface," *IEEE Transactions on Communications*, vol. 68, no. 12, pp. 7851–7866, 2020.

[18] M. Cui, G. Zhang, and R. Zhang, "Secure wireless communication via intelligent reflecting surface," *IEEE Wireless Communications Letters*, vol. 8, no. 5, pp. 1410–1414, 2019.

[19] X. Yu, D. Xu, Y. Sun, D. W. K. Ng, and R. Schober, "Robust and secure wireless communications via intelligent reflecting surfaces," *IEEE Journal on Selected Areas in Communications*, vol. 38, no. 11, pp. 2637–2652, 2020.

[20] Z. Chu, W. Hao, P. Xiao, D. Mi, Z. Liu, M. Khalily, J. R. Kelly, and A. P. Feresidis, "Secrecy rate optimization for intelligent reflecting surface assisted MIMO system," *IEEE Transactions on Information Forensics and Security*, vol. 16, pp. 1655–1669, 2021.

[21] S. Jiao, F. Fang, X. Zhou, and H. Zhang, "Joint beamforming and phase shift design in downlink UAV networks with IRS-assisted NOMA," *Journal of Communications and Information Networks*, vol. 5, no. 2, pp. 138–149, 2020.

[22] C. Huang, G. Chen, and K.-K. Wong, "Multi-agent reinforcement learning-based buffer-aided relay selection in IRS-assisted secure cooperative networks," *IEEE Transactions on Information Forensics and Security*, vol. 16, pp. 4101–4112, 2021.

[23] S. Fang, G. Chen, and Y. Li, "Joint optimization for secure intelligent reflecting surface assisted UAV networks," *IEEE Wireless Communications Letters*, vol. 10, no. 2, pp. 276–280, 2021.

[24] X. Li, C. Zhang, C. He, G. Chen, and J. A. Chambers, "Sum-rate maximization in IRS-assisted wireless power communication networks," *IEEE Internet of Things Journal*, vol. 8, no. 19, pp. 14959–14970, 2021.

[25] T. Wang, M.-A. Badiu, G. Chen, and J. P. Coon, "Outage probability analysis of RIS-assisted wireless networks with von mises phase errors," *IEEE Wireless Communications Letters*, pp. 1–1, 2021.

[26] P. Xu, G. Chen, Z. Yang, and M. D. Renzo, "Reconfigurable intelligent surfaces-assisted communications with discrete phase shifts: How many quantization levels are required to achieve full diversity?," *IEEE Wireless Communications Letters*, vol. 10, no. 2, pp. 358–362, 2021.

[27] L. Wei, C. Huang, G. C. Alexandropoulos, C. Yuen, Z. Zhang, and M. Debbah, "Channel estimation for RIS-empowered multi-user MISO wireless communications," *IEEE Transactions on Communications*, vol. 69, no. 6, pp. 4144–4157, 2021.

[28] H. Guo, Y.-C. Liang, J. Chen, and E. G. Larsson, "Weighted sum-rate maximization for reconfigurable intelligent surface aided wireless networks," *IEEE Transactions on Wireless Communications*, vol. 19, no. 5, pp. 3064–3076, 2020.

[29] C. Wang and R. Murch, "Adaptive downlink multi-user MIMO wireless systems for correlated channels with imperfect CSI," *IEEE Transactions on Wireless Communications*, vol. 5, no. 9, pp. 2435–2446, 2006.

[30] S. F. Zamanian, S. M. Razavizadeh, and Q. Wu, "Vertical beamforming in intelligent reflecting surface-aided cognitive radio networks," *IEEE Wireless Communications Letters*, pp. 1–1, 2021.

[31] G. Zhou, C. Pan, H. Ren, K. Wang, M. D. Renzo, and A. Nallanathan, "Robust beamforming design for intelligent reflecting surface aided MISO communication systems," *IEEE Wireless Communications Letters*, vol. 9, no. 10, pp. 1658–1662, 2020.

[32] J. Lyu and R. Zhang, "Hybrid active/passive wireless network aided by intelligent reflecting surface: System modeling and performance analysis," *IEEE Transactions on Wireless Communications*, vol. 20, no. 11, pp. 7196–7212, 2021.

[33] S. Hong, C. Pan, H. Ren, K. Wang, K. K. Chai, and A. Nallanathan, "Robust transmission design for intelligent reflecting surface-aided secure communication systems with imperfect cascaded CSI," *IEEE Transactions on Wireless Communications*, vol. 20, no. 4, pp. 2487–2501, 2021.

[34] Z. Wang, L. Liu, and S. Cui, "Channel estimation for intelligent reflecting surface assisted multiuser communications: Framework, algorithms, and analysis," *IEEE Transactions on Wireless Communications*, vol. 19, no. 10, pp. 6607–6620, 2020.

[35] L. You, J. Xiong, Y. Huang, D. W. K. Ng, C. Pan, W. Wang, and X. Gao, "Reconfigurable intelligent surfaces-assisted multiuser MIMO uplink transmission with partial CSI," *IEEE Transactions on Wireless Communications*, vol. 20, no. 9, pp. 5613–5627, 2021.

[36] T. Jiang, H. V. Cheng, and W. Yu, "Learning to reflect and to beamform for intelligent reflecting surface with implicit channel estimation," *IEEE Journal on Selected Areas in Communications*, vol. 39, no. 7, pp. 1931–1945, 2021.

[37] M.-M. Zhao, Q. Wu, M.-J. Zhao, and R. Zhang, "Two-timescale beamforming optimization for intelligent reflecting surface enhanced wireless network," in *2020 IEEE 11th Sensor Array and Multichannel Signal Processing Workshop (SAM)*, pp. 1–5, 2020.

[38] Z. Chen, J. Tang, X. Du, X. Y. Zhang, Q. Wu, and K.-K. Wong, "Joint location and channel error optimization for beamforming design for multi-RIS assisted MIMO system," in *2022 IEEE 12th Sensor Array and Multichannel Signal Processing Workshop (SAM)*, pp. 181–185, 2022.

[39] H. Liu, X. Yuan, and Y. J. A. Zhang, "Matrix-calibration-based cascaded channel estimation for reconfigurable intelligent surface assisted multiuser MIMO," *IEEE Journal on Selected Areas in Communications*, vol. 38, no. 11, pp. 2621–2636, 2020.

[40] T. E. Bogale and L. Vandendorpe, "Robust sum MSE optimization for downlink multiuser MIMO systems with arbitrary power constraint: Generalized duality approach," *IEEE Transactions on Signal Processing*, vol. 60, no. 4, pp. 1862–1875, 2012.

[41] Q. Zhang, C. He, and L. Jiang, "Per-stream MSE based linear transceiver design for MIMO interference channels with CSI error," *IEEE Transactions on Communications*, vol. 63, no. 5, pp. 1676–1689, 2015.

[42] N. Jindal, "MIMO broadcast channels with finite-rate feedback," *IEEE Transactions on Information Theory*, vol. 52, no. 11, pp. 5045–5060, 2006.

[43] K. Shen and W. Yu, "Fractional programming for communication systems—part II: Uplink scheduling via matching," *IEEE Transactions on Signal Processing*, vol. 66, no. 10, pp. 2631–2644, 2018.

[44] K. S. Yildirim, "Gradient descent algorithm inspired adaptive time synchronization in wireless sensor networks," *IEEE Sensors Journal*, vol. 16, no. 13, pp. 5463–5470, 2016.

[45] W. Feng, N. Zhao, S. Ao, J. Tang, X. Zhang, Y. Fu, D. K. C. So, and K.-K. Wong, "Joint 3D trajectory and power optimization for UAV-aided mmwave MIMO-NOMA networks," *IEEE Transactions on Communications*, vol. 69, no. 4, pp. 2346–2358, 2021.

[46] Q. Zhang and H. Li, "MOEA/D: A multiobjective evolutionary algorithm based on decomposition," *IEEE Transactions on Evolutionary Computation*, vol. 11, no. 6, pp. 712–731, 2007.

[47] M. R. Akdeniz, Y. Liu, M. K. Samimi, S. Sun, S. Rangan, T. S. Rappaport, and E. Erkip, "Millimeter wave channel modeling and cellular capacity evaluation," *IEEE Journal on Selected Areas in Communications*, vol. 32, no. 6, pp. 1164–1179, 2014.

[48] Y. Cao, T. Lv, and W. Ni, "Intelligent reflecting surface aided multi-user mmwave communications for coverage enhancement," in *2020 IEEE 31st Annual International Symposium on Personal, Indoor and Mobile Radio Communications*, pp. 1–6, 2020.

[49] "Further advancements for e-utra physical layer aspects (release 12)," *document 3GPP, TS 38.814*, 2020.

[50] Y. Sun, P. Babu, and D. P. Palomar, "Majorization-minimization algorithms in signal processing, communications, and machine learning," *IEEE Transactions on Signal Processing*, vol. 65, no. 3, pp. 794–816, 2017.